

Thesis for Master Degree

A Study on a Low-Cost Attitude and Heading
Estimation System for ROVs

Supervisor: Professor Ha Yun Su

2008-08

Korea Maritime University Graduate School

Department of Control and Instrumentation Engineering

Ngo Thanh Hoan

工學碩士學位論文

A Study on a Low-Cost Attitude and Heading
Estimation System for ROVs

指導教授 河 潤 秀

2008 年 8 月

韓國海洋大學校 大學院

制御計測工學科

Ngo Thanh Hoan

本 論文을 Ngo Thanh Hoan 의 工學碩士 學位論文으로 認准함.

委員長 工學博士 陳 康 奎



委 員 工學博士 金 煥 成



委 員 工學博士 河 潤 秀



2008 年 7 月

韓國海洋大學校 大學院

制御計測工學科

Ngo Thanh Hoan

Abstract

This thesis presents a methodology for designing a low-cost attitude and heading estimation system which is composed of three single-axis rate gyros, a tri-axis accelerometer, and a tri-axis magnetometer. Rate gyro sensor we have chosen is a small relatively inexpensive piezoelectric vibrating rate gyro originally developed for the automobile market and active suspension systems by Murata. It generates voltage output proportional to the angular velocity of the vehicle around the principal axis of the device. Accelerometer is a tri-axis digital output linear accelerometer developed by ST that includes a sensing element and an IC interface able to take the information from the sensing element and to provide the measured acceleration signals to the external world through an I2C/SPI interface. Magnetometer is an integrated tri-axis magnetic field sensing module manufactured by PNI. It is used to measure Earth's magnetic field. SPI interface allows easy access to its measurement parameters and resulting field measurement data. Output signals coming from these sensors are fused through two Kalman filters. One Kalman filter is used to estimate roll and pitch angles and the other is for heading angle estimation. By using this method, we have obtained attitude (roll and pitch angle) and heading information which are reliable over long period of time. Results from a set of simulation works have shown the performance of the presented method.

Acknowledgements

I am particularly grateful to people for their help, support, and encouragement during my study in Korea in last two years.

First of all, I would especially like to thank my supervisor, professor Ha Yun Su, who taught and gave me good advices on my research work at Korea Maritime University.

I want to give special thanks to Mr. Park Seung Soo and Mr. Oh Young Seock for their fully support for my study and living in Korea.

I am grateful to professors who taught me: professor Jin Gang Gyoo, professor Kim Jong Hwa, and professor Yu Yung Ho and other professors.

I would like to thank the people at SonarTech Co., Ltd. including: Mr. Kim Young Il, Mr. Ko Yun Ho, Mr. Park Dong Jin, Mr. Choi Young Ho, Mr. Yun Yang Ho and many others. It has been a privilege to work with them.

I would also like to thank Vietnamese friends at Korea Maritime University including: Nguyen Duy Anh, Tran Thanh Ngon, Do HUU Hien, Le Quynh Lam, Vu Manh Dat, Nguyen Hoang Phuong Khanh, Nguyen Tien Thanh, Nguyen Kim Bao.

I want to thank Korean, Myanmar, Chinese, and Japanese friends including: Kim Min Jung, Aung Khaing Nyi and many others. They are really friendly and kind-hearted.

Finally, I would like to express my deep gratitude to my parents for their love, patience and support.

Contents

Abstract	ii
Acknowledgements	iii
Contents	iv
List of Figures	v
Chapter 1 Introduction.....	1
Chapter 2 Theoretical Background.....	5
2.1 Attitude and heading representation	5
2.2 Attitude and heading determination using rate gyros	8
2.3 Attitude determination using accelerometers.....	11
2.4 Heading determination using magnetometer	14
Chapter 3 Design Attitude and Heading Estimation System.....	17
3.1 Hardware design process	17
3.1.1 Rate gyro sensor.....	19
3.1.2 Tri-axis accelerometer.....	22
3.1.3 Tri-axis magnetic sensor	24
3.2 Data fusion algorithm	25
3.2.1 Attitude estimator.....	25
3.2.2 Heading estimator	29
Chapter 4 Simulation Studies	32
Chapter 5 Conclusions.....	39
References.....	40

List of Figures

Figure 1.1	Attitude & Heading Reference System (AHRS).....	1
Figure 1.2	Applications of AHRS.....	1
Figure 2.1	Body frame.	6
Figure 2.2	Euler angle sequence.	7
Figure 2.3	The Euler angles calculated using rate gyro measurements.	10
Figure 2.4	Position vector with respect to reference frame.	11
Figure 2.5	Attitude angles calculated using accelerometer measurement.	13
Figure 2.6	The Earth's magnetic vector.	14
Figure 2.7	Heading angle calculated using magnetometer measurement.	16
Figure 3.1	Attitude and heading estimation system block schematic.	17
Figure 3.2	Prototype board in development process.	18
Figure 3.3	Rate gyro sensor output characteristic.	19
Figure 3.4	Rate gyros configuration.	19
Figure 3.5	Definition of axis rotations.	20
Figure 3.6	Rate gyro signal conditioning principle.....	20
Figure 3.7	Rate gyro signal conditioning circuit.....	21
Figure 3.8	Accelerometer LIS3LV03DQ.	23
Figure 3.9	Tri-axis magnetic field sensing module MicroMag3.	24
Figure 3.10	Data fusion algorithm.	25
Figure 4.1	Acceleration, velocity of the body and non-acceleration detect signal.	33
Figure 4.2	Normalized magnitude of Earth's magnetic field, error in dip angle, and homogeneous & undisturbed Earth's magnetic field detect signal.	34
Figure 4.3	Roll, pitch, and yaw angles. Solid lines denote true values and dashed estimated.	35
Figure 4.4	Errors in estimated roll, pitch, and yaw angles.	36
Figure 4.5	Elements of diagonal of estimated error covariance matrix of the attitude estimator.	37
Figure 4.6	Estimated error variance of the heading estimator.	38

Chapter 1 Introduction

Attitude and heading estimation is one of important steps in the design of an ROV since estimated angles are used in the lowest control loop to stabilize the vehicle. Commercially available products for this task provide good quality but tend to be expensive and heavy (Figure 1.1). They are usually used in applications such as: aircraft, military vehicle, satellite (Figure 1.2). In applications where budget is small like ours, developing a low-cost attitude and heading estimation system while still providing high accuracy is necessary.



Figure 1.1 Attitude & Heading Reference System (AHRS).



Figure 1.2 Applications of AHRS.

There are several kinds of sensors from which we can obtain attitude (roll and pitch) and heading information. For attitude measurement, following sensors are most commonly used:

- The first is inclinometer. The sensor output is proportional to the tilt angle with respect to the field of gravity. This kind of sensor, however, has slow response and therefore can't be used alone in attitude estimation system.
- The second is rate gyro sensor. The sensor measures the rate of rotation. To obtain angle of orientation, we have to integrate sensor signal. Thus, even small errors in the rate information can lead to drift in calculated angle.
- The third is accelerometer which relates the body to the gravity acceleration vector. The problem is the sensor is sensitive to translational accelerations and should only be used during phases of low accelerations.

For heading measurement, we can integrate gyro signal but it also leads to drift as in attitude estimation case. Another sensor can be used is magnetometer which measure magnetic field of the Earth. Although the sensor itself has become very accurate and compact, magnetic field sensing is still very erroneous because of environmental factors.

To address the above problems, we need a fusion method to integrate measurements coming from these kinds of sensors. In [1], Baerveldt and Klang have analyzed the problem of fusing inclinometers and gyros using linear complementary filter and frequency domain analysis. A similar filter has been recently used by Klaus Loffler et al in [2] for estimating attitude of a Biped robot. But they only considered planar motions. Vaganay, Aldon, Fournier [3] proposed an attitude estimation system for a mobile robot using Extended Kalman filter to fuse data from accelerometers and gyroscopes. This method, however, requires that

non gravitational acceleration has to be removed from the accelerometer output by using odometry. It is, therefore, inapplicable to ROV. Another Extended Kalman filter was presented by Barshan and Durrant-Whyte in [4][5] where error model of gyroscope was constructed for estimating the heading angle of the robot. They showed that the error in heading estimation can be improved at least by factor of 5 if an adequate error model is supplied. Nevertheless, they found that additional information from some absolute sensing mechanism is necessary to overcome long-term drift. In [6], Ojeda and Borenstein introduced a new Fuzzy Logic Expert rule-based navigation method for fusing data from multiple low- to medium-cost gyroscopes and accelerometers in order to estimate the attitude and heading of a mobile robot. But encoder information is required to resolve the “standing and moving” ambiguity. More recently, in [7], Rehbinder and Hu developed a switching state estimator for sensing attitude in three dimensions. Their approach combines gyro and acceleration measurements when robot is under low acceleration state, and switches the estimator rely mostly on the gyro signal when under high acceleration state. The estimator has been successfully implemented on a walking robot; however, only attitude angles were estimated. Our approach combines the above estimator and another estimator which result in not only attitude angles but also heading angle.

In our proposed method, two state estimators have been incorporated. The first one is based on the estimator developed by Rehbinder and Hu and dedicates to attitude estimation. The second one uses the first one’s result to transform the Earth’s magnetic field vector measured by magnetometers in body frame to inertial frame. Heading angle is then calculated from the transformed Earth’s magnetic field vector and is fused with gyro data to reduce noise in heading estimation. Both the estimator is Kalman-based fusion algorithm. Tests have shown that we obtained attitude (roll and pitch angles) and heading information which is reliable over long period of time.

The thesis is organized as follows. Chapter 2 gives a brief overview of background knowledge. In Chapter 3, the attitude and heading estimation system is presented. In Chapter 4, simulation results illustrate performance of the proposed approach. Finally, Chapter 5 summarizes conclusions of the presented works.

Chapter 2 Theoretical Background

2.1 Attitude and heading representation

Before describing the attitude and heading estimation system, we should agree on how attitude and heading angles are represented. Consider a rigid body rotating and translating in the inertial space. Our aim is to estimate attitude and heading of the rigid body in the inertial space. To do this, three right-handed orthogonal coordinate frames are defined:

- Navigation frame, n -frame. It was used as reference frame. The n -frame has its origin at some point fixed in the body where the measurement system is located, and x_n -axis points North, y_n -axis points East, and z_n -axis points vertical down (to the Earth's centre). It is so called North-East-Down (NED) frame.
- Body frame, b -frame. It has the same origin as navigation frame's, the x_b -axis (roll) points forward, y_b -axis (pitch) points to the right, and the z_b -axis (yaw) points downward (Figure 2.1).
- Horizontal frame, h -frame. The b -frame is called the h -frame when their attitude angles are zeros.

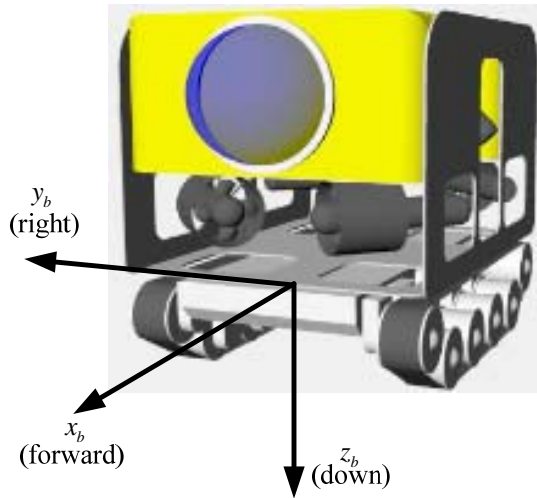


Figure 2.1 Body frame.

Various mathematical representations can be used to define the attitude and heading of a body frame with respect to a reference frame such as: direction cosine matrix, Euler angles, quaternions. In this work, Euler angle representation is utilized because of its intuitive nature and popularity despite drawback such as singularities. According to Euler's theorem, we can specify the orientation of the body frame relative to the reference frame by three angles (ψ, θ, ϕ) , known as Euler angles, and obtained by three successive rotations about different axes, known as Euler angle sequence. Following Euler angle sequence is chosen to transform reference to body frame:

- Rotate through angle ψ (yaw) about reference z -axis,
- Rotate through angle θ (pitch) about new y -axis,
- Rotate through angle ϕ (roll) about new x -axis.

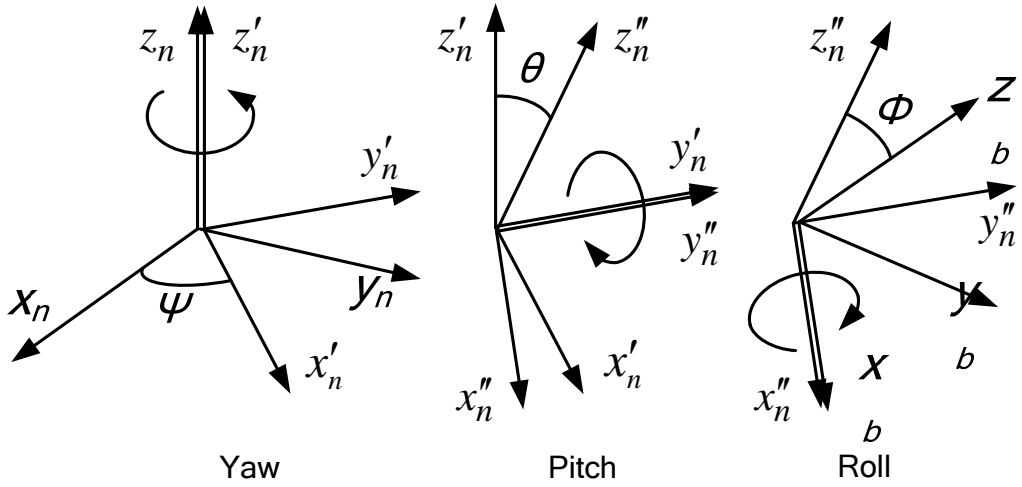


Figure 2.2 Euler angle sequence.

Yaw and pitch angles define attitude while roll angle defines heading of the b -frame with respect to the n -frame.

The three rotations may be expressed mathematically by following three separate direction cosine matrices, respectively:

$$\text{rotate } \psi \text{ about } z\text{-axis, } \mathbf{C}_z = \begin{bmatrix} \cos \psi & \sin \psi & 0 \\ -\sin \psi & \cos \psi & 0 \\ 0 & 0 & 1 \end{bmatrix} \quad (2.1)$$

$$\text{rotate } \theta \text{ about } y\text{-axis, } \mathbf{C}_y = \begin{bmatrix} \cos \theta & 0 & -\sin \theta \\ 0 & 1 & 0 \\ \sin \theta & 0 & \cos \theta \end{bmatrix} \quad (2.2)$$

$$\text{rotate } \phi \text{ about } x\text{-axis, } \mathbf{C}_x = \begin{bmatrix} 1 & 0 & 0 \\ 0 & \cos \phi & \sin \phi \\ 0 & -\sin \phi & \cos \phi \end{bmatrix} \quad (2.3)$$

Thus, a transformation from reference to body axes may be expressed as product of these three separate transformations as follows:

$$\begin{aligned} \mathbf{C}_n^b &= \mathbf{C}_x \mathbf{C}_y \mathbf{C}_z \\ &= \begin{bmatrix} \cos\psi \cos\theta & \sin\psi \cos\theta & -\sin\theta \\ -\sin\psi \cos\phi + \cos\psi \sin\theta \sin\phi & \cos\psi \cos\phi + \sin\psi \sin\theta \sin\phi & \cos\theta \sin\phi \\ \sin\psi \sin\phi + \cos\psi \sin\theta \cos\phi & \sin\psi \sin\theta \cos\phi - \cos\psi \sin\phi & \cos\theta \cos\phi \end{bmatrix} \end{aligned} \quad (2.4)$$

Similarly, the inverse transformation from body to reference axes is given by:

$$\mathbf{C}_b^n = (\mathbf{C}_n^b)^T = (\mathbf{C}_z)^T (\mathbf{C}_y)^T (\mathbf{C}_x)^T \quad (2.5)$$

2.2 Attitude and heading determination using rate gyros

Rates of rotation of the body frame relative to the reference frame can be expressed in terms of the derivatives of the Euler angles $(\dot{\psi}, \dot{\theta}, \dot{\phi})$ called ‘‘Euler rates’’.

Specifically, Euler rates and rate gyros are related by [8]:

$$\begin{bmatrix} \dot{\phi} \\ \dot{\theta} \\ \dot{\psi} \end{bmatrix} = \begin{bmatrix} 1 & \sin\phi \tan\theta & \cos\phi \tan\theta \\ 0 & \cos\phi & -\sin\phi \\ 0 & \frac{\sin\phi}{\cos\theta} & \frac{\cos\phi}{\cos\theta} \end{bmatrix} \begin{bmatrix} \omega_x \\ \omega_y \\ \omega_z \end{bmatrix} \quad (2.6)$$

where ω_x , ω_y , and ω_z are the rates of rotation of the body around the respective axes of the body frame and are measured using rate gyros.

If initial Euler angles and rate gyros data are known, we can calculate Euler angles by solving the above equation using numerical integration. However, as mentioned above, there always exist errors in rate gyros such as axis misalignment,

fixed bias, drift bias, and so on. These errors cause the integration result to drift from the true values as a function of time.

The existence of drift is verified by simulation in MATLAB. In the simulation, the body is initially at $\phi = -\pi/34$, $\theta = 0$, and $\psi = 0$ and rotating about x_b -axis at angular velocity $\omega_x = 0.27 \times \sin(2 \times \pi \times 0.23 \times t) + 0.03 \times \sin(2 \times \pi \times 0.11 \times t) + 0.01 \times \sin(2 \times \pi \times 0.593 \times t)$ [rad/s] and about y_b -axis at angular velocity $\omega_y = 0.21 \times \cos(2 \times \pi \times 0.14 \times t) + 0.03 \times \cos(2 \times \pi \times 0.39 \times t) + 0.02 \times \cos(2 \times \pi \times 0.12 \times t)$ [rad/s] while $\omega_z = 0$ [rad/s]. From the above angular velocities, solve Equation (2.6) numerically using the fourth-order Runge-Kutta method, we obtain Euler angles. Because the Euler angles are calculated from true angular velocities, we consider them as reference Euler angles. Rate gyro measurements can be simulated by adding zero-mean Gaussian white noise with $\sigma = 0.001$ [rad/s] and offset 0.005 [rad/s] to the above angular velocities. From the rate gyro measurements, solve Equation (2.6) again, we obtain Euler angles considered as measured values. In Figure 2.3, we can see that measured Euler angles diverge from reference Euler angles.

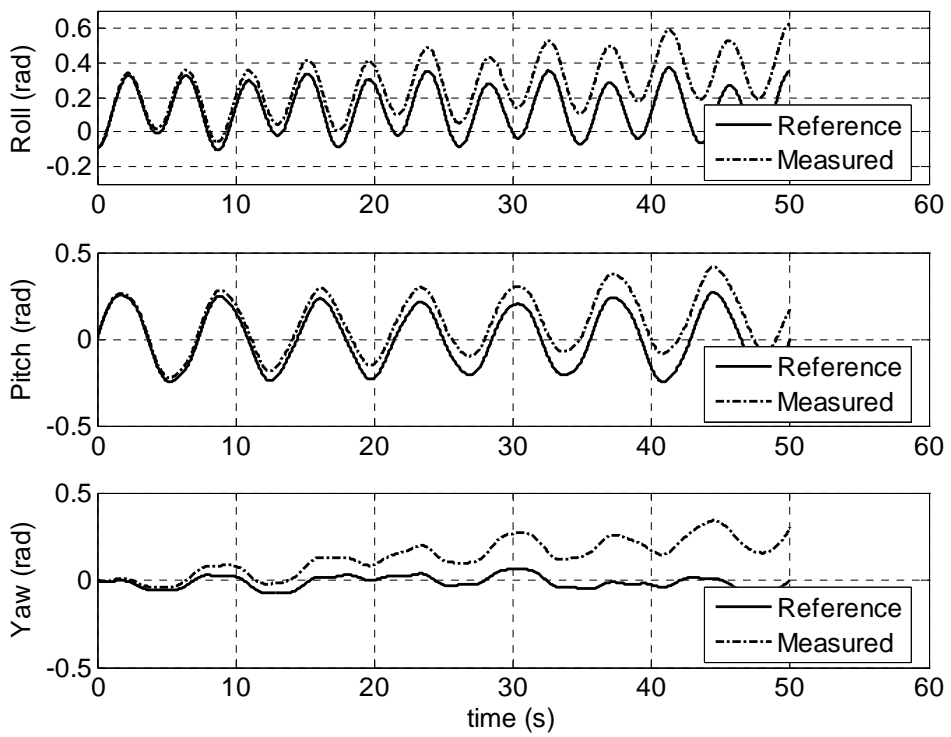


Figure 2.3 The Euler angles calculated using rate gyro measurements.

2.3 Attitude determination using accelerometers

The acceleration of P as shown in Figure 2.4 with respect to n -frame is defined by:

$$\mathbf{a}_n = \left. \frac{d^2 \mathbf{r}}{dt^2} \right|_n \quad (2.7)$$

Since the accelerometer in this application is fixed to the body, it provides a measurement of specific force acting at point P in the b -frame, denoted $\mathbf{f}_b = [f_{xb} \ f_{yb} \ f_{zb}]^T$. We have [8]:

$$\mathbf{f}_b = \mathbf{C}_n^b (\mathbf{a}_n - \mathbf{g}_n) \quad (2.8)$$

where $\mathbf{a}_n = [a_{xn} \ a_{yn} \ a_{zn}]^T$ is the acceleration of the body in the n -frame and $\mathbf{g}_n = [0 \ 0 \ g]^T$ is the mass attraction gravitation vector with $g = 9.81 \text{ [m/s}^2\text{]}$.

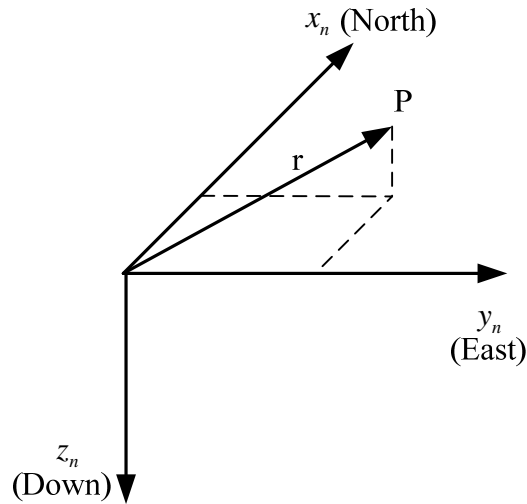


Figure 2.4 Position vector with respect to reference frame.

Denote that \mathbf{x} is the third column of \mathbf{C}_n^b , rearranging Equation (2.8), we have:

$$\mathbf{f}_b = \mathbf{C}_n^b \mathbf{a}_n - \mathbf{x}g \quad (2.9)$$

When the body is not accelerating, $\mathbf{a}_n = \mathbf{0}$, we have:

$$\mathbf{f}_b = -\mathbf{x}g \quad (2.10)$$

From Equation (2.10), attitude angles are calculated as:

$$\theta_{ACC} = \sin^{-1}\left(\frac{f_{xb}}{g}\right), \quad \phi_{ACC} = \sin^{-1}\left(\frac{-f_{yb}}{g \cos \theta_{ACC}}\right) \quad (2.11)$$

where θ_{ACC} and ϕ_{ACC} are pitch and roll angles calculated using accelerometer data, respectively. It should be noted that the attitude determination using Equation (2.11) is true only if the body is not accelerating. When the body accelerates, attitude angles calculated by using this method are invalid.

The attitude angles calculation using accelerometer data is verified by simulation in MATLAB. In the simulation, the body is initially at $\phi = -\pi/34$, $\theta = 0$, and $\psi = 0$ and rotating about x_b -axis at angular velocity $\omega_x = 0.27 \times \sin(2 \times \pi \times 0.23 \times t) + 0.03 \times \sin(2 \times \pi \times 0.11 \times t) + 0.01 \times \sin(2 \times \pi \times 0.593 \times t)$ [rad/s] and about y_b -axis at angular velocity $\omega_y = 0.21 \times \cos(2 \times \pi \times 0.14 \times t) + 0.03 \times \cos(2 \times \pi \times 0.39 \times t) + 0.02 \times \cos(2 \times \pi \times 0.12 \times t)$ [rad/s] while $\omega_z = 0$ [rad/s]. From the above angular velocities, solve Equation (2.6) numerically using the fourth-order Runge-Kutta method, we obtain Euler angles. Because the Euler angles are calculated from true angular velocities, we consider them as reference Euler angles. From Euler angles and accelerations, specific force \mathbf{f}_b is obtained by solving Equation (2.8). Accelerometer measurement can be simulated by adding zero-mean Gaussian white noise with $\sigma = 0.001g$ to components of the above specific force. From the accelerometer measurement, solve Equation (2.11), we obtain attitude angles considered as measured values. In Figure 2.5, we can see that measured pitch angle diverge from

reference pitch angle when the body accelerates.

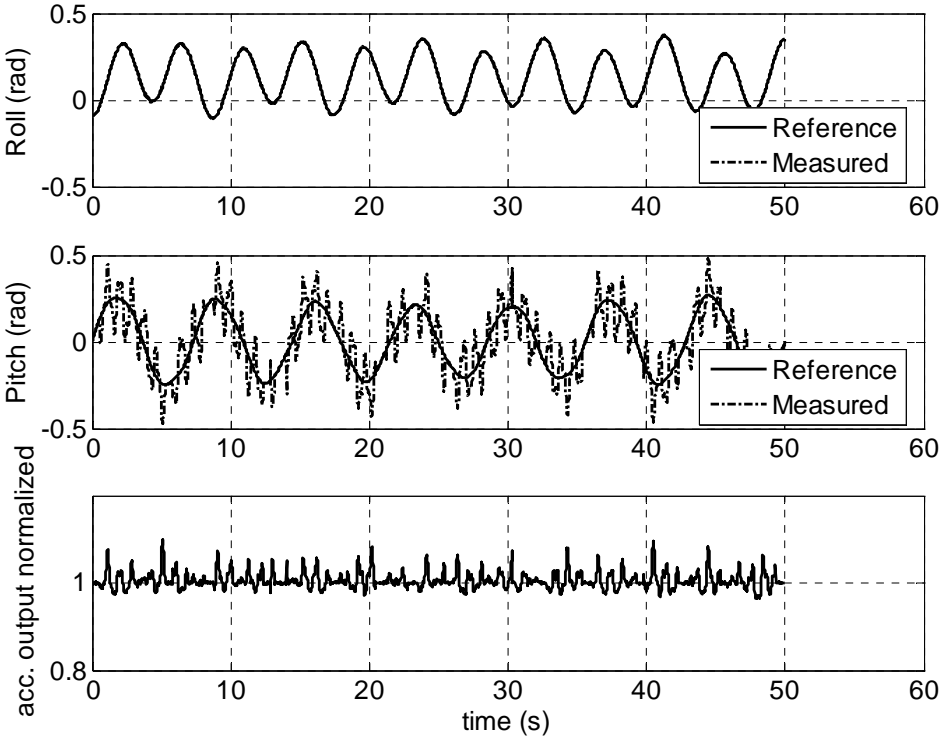


Figure 2.5 Attitude angles calculated using accelerometer measurement.

2.4 Heading determination using magnetometer

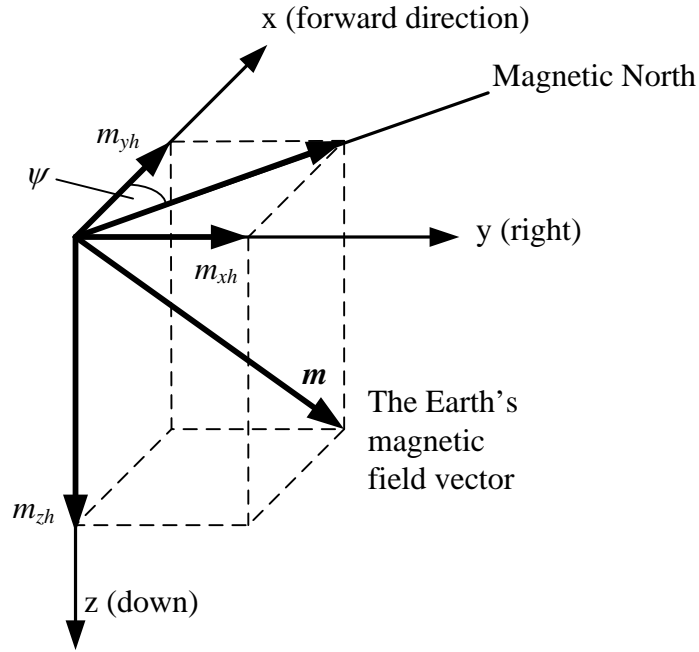


Figure 2.6 The Earth's magnetic vector.

To determine heading angle ψ from the Earth's magnetic field vector \mathbf{m} components of the vector in h -frame m_{xh} and m_{yh} have to be known (Figure 2.6). These components are measured by magnetometer fixed to h -frame. However, in this application, the magnetic field sensor is fixed to the b -frame, it provides a measurement of the Earth's magnetic field vector in the b -frame, denoted $\mathbf{m}_b = [m_{xb} \ m_{yb} \ m_{zb}]^T$. Hence the measured vector has to be transformed into h -frame. This technique is often referred to as *electronical gimbaling*. Denote $\mathbf{m}_h = [m_{xh} \ m_{yh} \ m_{zh}]^T$ is the Earth's magnetic field vector expressed in h -frame, we have [9]:

$$\begin{bmatrix} m_{xh} \\ m_{yh} \\ m_{zh} \end{bmatrix} = \begin{bmatrix} \cos \theta & \sin \phi \sin \theta & \cos \phi \sin \theta \\ 0 & \cos \phi & -\sin \phi \\ -\sin \theta & \sin \phi \cos \theta & \cos \phi \cos \theta \end{bmatrix} \begin{bmatrix} m_{xb} \\ m_{yb} \\ m_{zb} \end{bmatrix} \quad (2.12)$$

Finally, heading angle is computed as:

$$\psi_{MAG} = \text{arctg} \left(-\frac{m_{yh}}{m_{xh}} \right) \quad (2.13)$$

where ψ_{MAG} is yaw angle calculated using magnetometer data. However, the heading angle determination method above is valid only in the homogeneous and undisturbed Earth's magnetic field. When Earth's magnetic field is non-homogeneous and disturbed, the method is very erroneous.

The above method is verified by simulation in MATLAB. In the simulation, the body is initially at $\phi = -\pi/34$, $\theta = 0$, and $\psi = 0$ and rotating about x_b -axis at angular velocity $\omega_x = 0.27 \times \sin(2 \times \pi \times 0.23 \times t) + 0.03 \times \sin(2 \times \pi \times 0.11 \times t) + 0.01 \times \sin(2 \times \pi \times 0.593 \times t)$ [rad/s] and about y_b -axis at angular velocity $\omega_y = 0.21 \times \cos(2 \times \pi \times 0.14 \times t) + 0.03 \times \cos(2 \times \pi \times 0.39 \times t) + 0.02 \times \cos(2 \times \pi \times 0.12 \times t)$ [rad/s] while $\omega_z = 0$ [rad/s]. From the above angular velocities, solve Equation (2.6) numerically using fourth-order Runge-Kutta method, we obtain Euler angles. Because the Euler angles are calculated from true angular velocities, we consider them as reference. From these angles, we obtain rotation matrix which transforms the Earth's magnetic field vector in n -frame \mathbf{m}_n to a vector in b -frame \mathbf{m}_b . To simulate non-homogeneous and disturbed Earth's magnetic field, a noise vector is added to the vector \mathbf{m}_n after each 5 seconds. It makes normalized magnitude of \mathbf{m}_n change after each 5 seconds (Figure 2.7). Magnetometer measurement can be simulated by adding zero-mean Gaussian white noises with $\sigma = 0.1\%$ of magnitude of the Earth's magnetic field vector to components of \mathbf{m}_b . From the magnetometer measurement, solve Equation (2.12) and (2.13), we obtain heading angle considered as measured value. In Figure 2.7, we can see that error of measured heading angle using magnetometer measurement is small when Earth's magnetic field is homogeneous and vice versa.

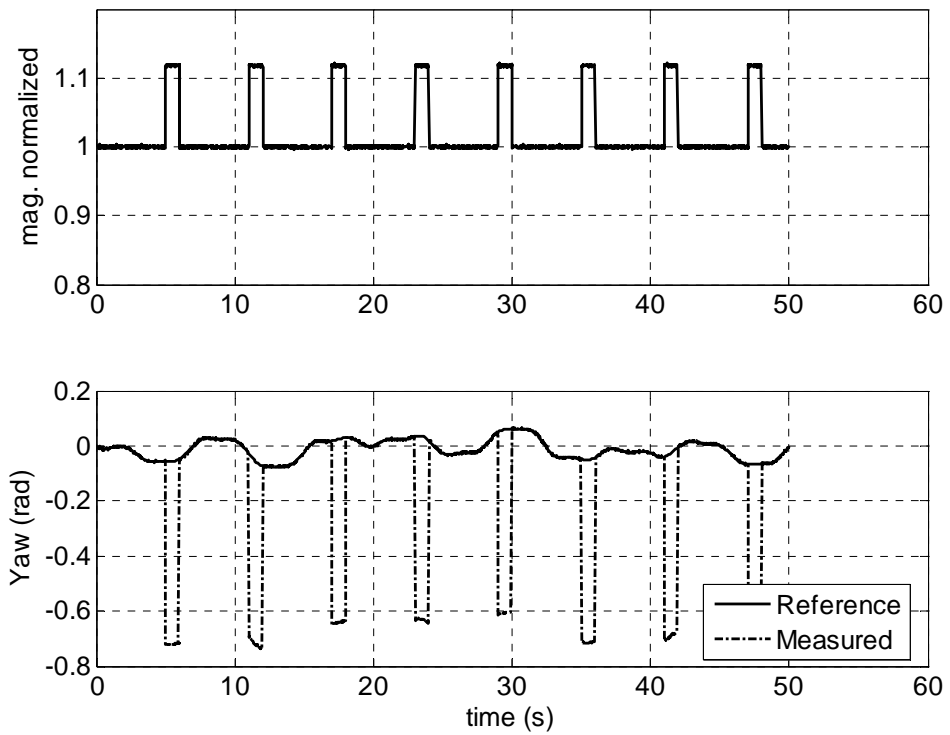


Figure 2.7 Heading angle calculated using magnetometer measurement.

Chapter 3 Design Attitude and Heading Estimation System

As seen in the previous chapter, each method which determines attitude and heading has advantages and disadvantages. The method using rate gyro has good performance in short time but results in drift after long period. Meanwhile, the method using accelerometer has good performance when the body is under non-acceleration state but is invalid when the body is accelerating. The method using magnetometer has no drift but is valid only in the homogeneous and undisturbed Earth's magnetic field. Therefore, a fusion method is necessary to exploit advantages of each method. A proposed fusion method will be presented in following Sections.

3.1 Hardware design process

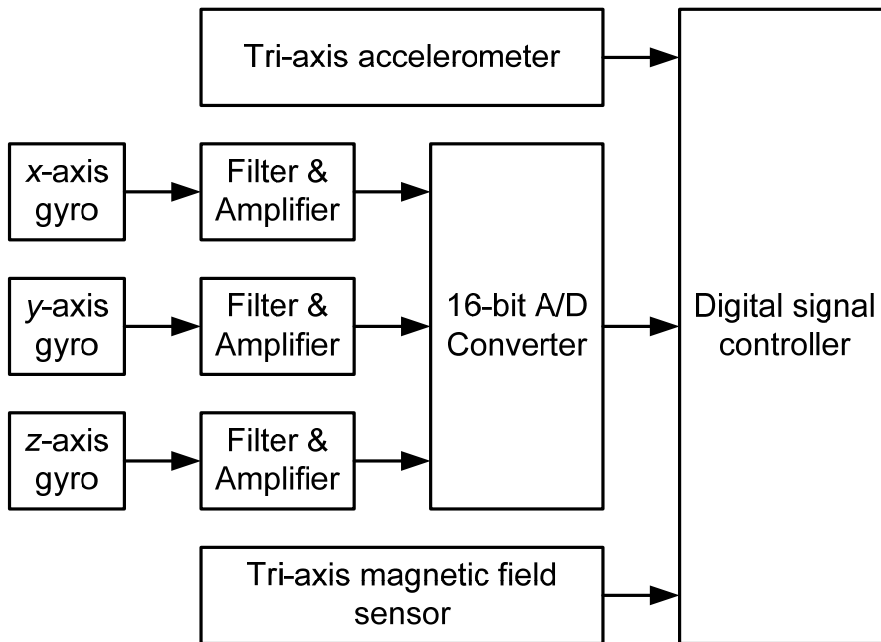


Figure 3.1 Attitude and heading estimation system block schematic.

In our approach, three single-axis rate gyros ENC-03M, a tri-axis accelerometer LIS3LV02DQ, and a tri-axis magnetic field sensing module MicroMag3 are used. Signals coming from the sensors are processed by digital signal controller TMS320F2812 where data fusion algorithm is implemented (Figure 3.1). A prototype PCB is developing as illustrated in Figure 3.2.



Figure 3.2 Prototype board in development process.

3.1.1 Rate gyro sensor

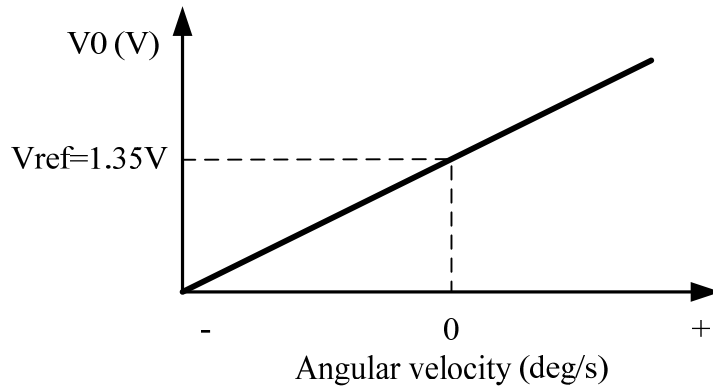


Figure 3.3 Rate gyro sensor output characteristic.

Rate gyro adopted is low-cost single-axis ENC-03M manufactured by Murata. The maximum angular velocity that can be measured is ± 300 [deg/s]. At angular velocity $\omega = 0$, sensor output $V_0 = V_{ref} = 1.35$ [V], as illustrated in Figure 3.3. Its sensitivity is 0.67 [mV/deg/s].

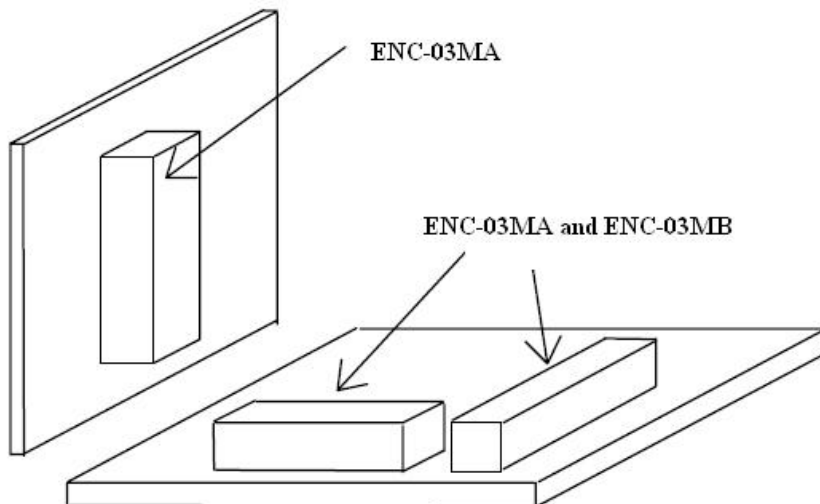


Figure 3.4 Rate gyros configuration.

There are two types of ENC-03M rate gyro. One is ENC-03MA and the other is ENC-03MB. They have the same specifications but use different frequencies to avoiding mutual interference when mounted on the same system. So when two axes are to be detected, two different types should be used. In our system, however, three axes sensing is required. Thus two ENC-03MA type rate gyros and one ENC-03MB type rate gyro are used where the first ENC-03MA type rate gyro and the ENC-03MB type rate gyro are installed on the same PCB while the second ENC-03MA type rate gyro is installed on a separate PCB, as indicated in Figure 3.4. Note that *b*-frame is right-handed axis sets in which positive rotations about each axis are taken to be in a clockwise direction looking along the axis from the origin. Therefore, rate gyros should be mounted on PCB so that their positive rotations match with positive rotations of three axes of *b*-frame (Figure 3.5).

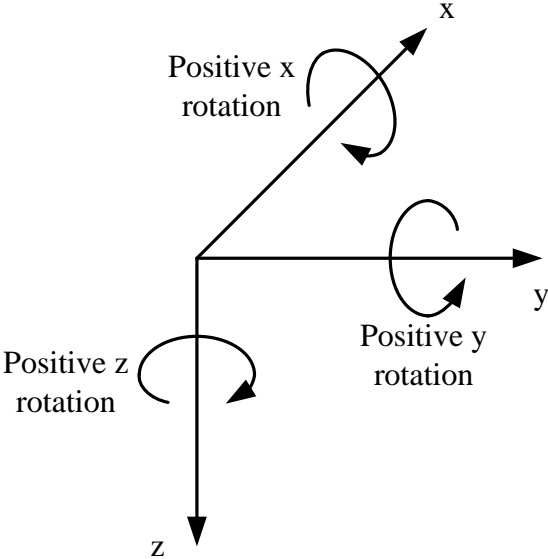


Figure 3.5 Definition of axis rotations.

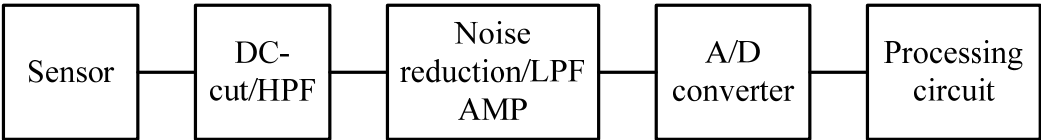


Figure 3.6 Rate gyro signal conditioning principle.

To reduce the effect of temperature drift (due to change of ambient temperature), a high pass filter must be connected to sensor output to eliminate DC component. To suppress output noise component around 22-25k [Hz] (resonant frequency of sensor element), a low pass filter which has higher cut-off frequency than required response frequency must be connected to sensor output (Figure 3.6).

In our work, following signal conditioning circuit was designed as depicted in Figure 3.7.

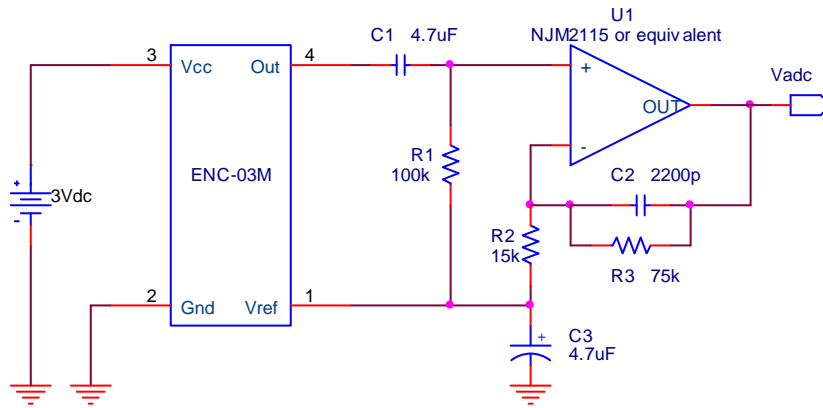


Figure 3.7 Rate gyro signal conditioning circuit.

High-pass filter's cut-off frequency:

$$f_1 = \frac{1}{2 \times \pi \times R1 \times C1} = \frac{1}{2 \times \pi \times 100k \times 4.7\mu} = 0.34 \text{ [Hz]} \quad (3.1)$$

Low-pass filter's cut-off frequency:

$$\begin{aligned} f_2 &= \frac{1 + (R2/R3)}{2 \times \pi \times R3 \times C2 \times \sqrt{1 + 2 \times (R2/R3) - (R2/R3)^2}} \\ &= \frac{1 + (15/75)}{2 \times \pi \times 75k \times 2200p \times \sqrt{1 + 2 \times (15/75) - (15/75)^2}} \\ &= 0.99 \text{ k [Hz]} \end{aligned} \quad (3.2)$$

Gain:

$$A = 1 + \frac{R3}{R2} = 1 + \frac{75}{15} = 6 \quad (3.3)$$

Angular velocity is calculated as follows:

$$\omega = \frac{Vadc - Vref}{A \times 0.67 \times 10^{-3}} \text{ [deg/s]} \quad (3.4)$$

where $Vadc$ is voltage measured at output of Op-amp U1 when angular velocity is ω and $Vref$ is voltage measured at output of Op-amp U1 when angular velocity is zero.

Compute angular velocity for each axis, finally we have $\boldsymbol{\omega} = [\omega_x \ \omega_y \ \omega_z]^T$.

3.1.2 Tri-axis accelerometer

For acceleration measurement, digital output tri-axis accelerometer LIS3LV02DQ is used (Figure 3.8). It includes a sensing element and an IC interface able to take the information from the sensing element and to provide the measured acceleration signals to the external world through and I2C/SPI serial interface. It has a user selectable full scale of +/-2g, +/-6g and it is capable of measuring acceleration over a bandwidth of 640 [Hz] for all axes. The device bandwidth may be selected accordingly to the application requirements. A self-test capability allows the user check the functioning of the system.

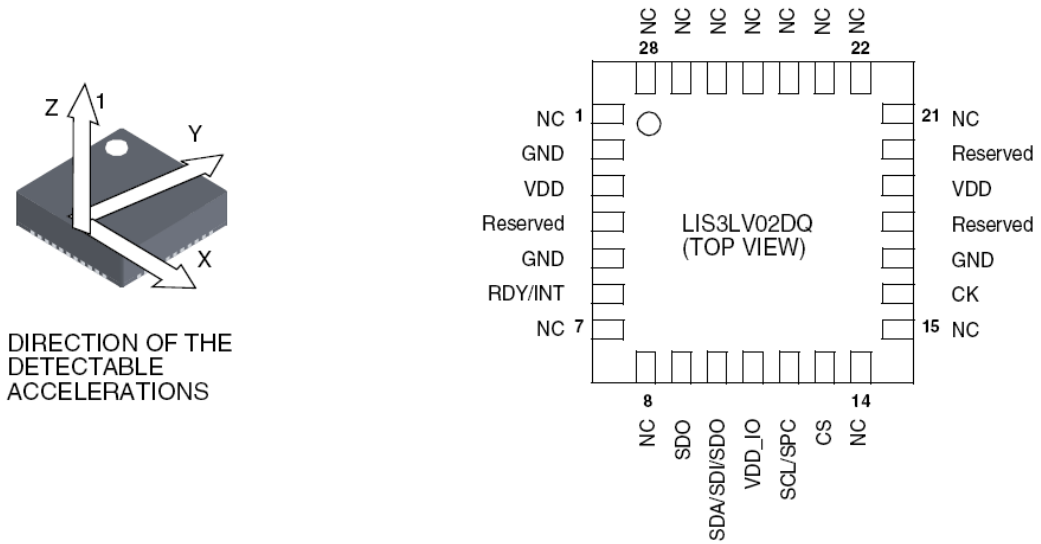


Figure 3.8 Accelerometer LIS3LV03DQ.

In our application, $\pm 2g$ full scale was selected. At this full scale, sensitivity is 1024 LSb/g. Hence specific force $\mathbf{f}_b = [f_{x_b} \ f_{y_b} \ f_{z_b}]^T$ is calculated as follows:

$$\mathbf{f}_b = \frac{\mathbf{OUT}}{1024} g \quad (3.5)$$

where $\mathbf{OUT} = [OUTX \ OUTY \ OUTZ]^T$ with $OUTX$, $OUTY$, and $OUTZ$ are values which are read in $OUTX$, $OUTY$, and $OUTZ$ registers of the accelerometer through I2C/SPI interface, respectively. In our work, when mounted on PCB, Y and Z axis of the accelerometer have reverse direction with y_b -axis and z_b -axis of b -frame. Thus $OUTY$ and $OUTZ$ must be reversed signs to provide measurements in b -frame.

3.1.3 Tri-axis magnetic sensor

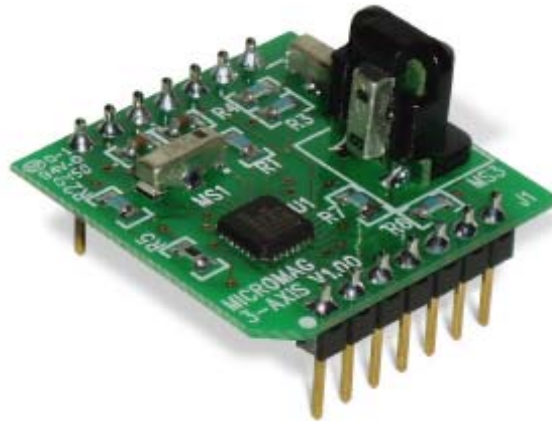


Figure 3.9 Tri-axis magnetic field sensing module MicroMag3.

For the Earth's magnetic field measurement, PNI's tri-axis magnetic field sensing module, MicroMag3, is used (Figure 3.9). It combines PNI Corporation's patented Magneto-Inductive (MI) sensors and measurement circuit technology for unparalleled cost effectiveness and performance. The microprocessor compatible SPI interface allows easy access to the MicroMag3's measurement parameters and resulting field measurement data. Advantages include 3 [V] operation for compatibility with new systems, low power consumption, large signal noise immunity under all conditions, and a large dynamic range. Resolution and field measurement range are software configurable for a variety of applications. The measurement is very stable over temperature and inherently free from offset drift.

The MicroMag3 magnetic sensor operates as an oscillator circuit composed of the internal sensors, bias resistors, digital gates and a comparator. Only one sensor can be measured at a time. The user sends a command byte to the MicroMag3 through the SPI port specifying the sensor axis to be measured and the sensor will return the result in a 16-bit 2's complement format.

3.2 Data fusion algorithm

Sensor's signals are processed by two Kalman-based estimators. The first estimator estimates roll and pitch angle by fusing rate gyros and accelerometer data. The second one estimates yaw angle by fusing rate gyros and magnetic field sensor. Notice that in the second estimator, magnetic field sensor measured in the body frame is compensated for roll and pitch (estimated by the first estimator) to obtain it's transformed in the h -frame before being fused with rate gyros data. Whole system is illustrated in Figure 3.10.

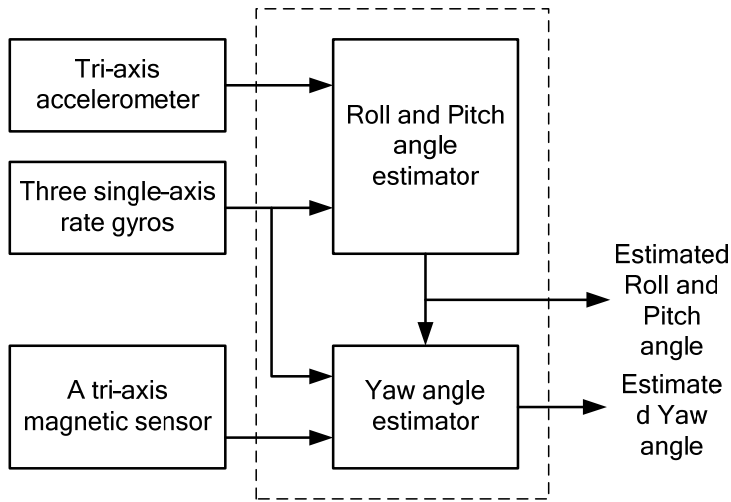


Figure 3.10 Data fusion algorithm.

3.2.1 Attitude estimator

The direction cosine matrix C_b^n can be calculated from angular measurements provided by the gyroscopes using following equation [8]:

$$\dot{C}_b^n = C_b^n \Omega \quad (3.6)$$

where Ω is the skew matrix

$$\mathbf{\Omega} = \begin{pmatrix} 0 & -\omega_z & \omega_y \\ \omega_z & 0 & -\omega_x \\ -\omega_y & \omega_x & 0 \end{pmatrix}$$

which is formed from the vector $\boldsymbol{\omega} = [\omega_x \ \omega_y \ \omega_z]^T$

From Equation (3.6), direction cosine matrix \mathbf{C}_n^b may be calculated:

$$\dot{\mathbf{C}}_n^b = (\dot{\mathbf{C}}_b^n)^T = (\mathbf{\Omega})^T (\mathbf{C}_b^n)^T = (\mathbf{\Omega})^T \mathbf{C}_n^b \quad (3.7)$$

Note that the third column of \mathbf{C}_n^b is independent of yaw. If that column could be estimated, then it would be possible to extract pitch and roll from it [7]. Denote \mathbf{x} is the third column of \mathbf{C}_n^b , from Equation (3.7) we have:

$$\dot{\mathbf{x}} = (\mathbf{\Omega})^T \mathbf{x} \quad (3.8)$$

For notational simplicity, we redefine $\mathbf{S}(\boldsymbol{\omega}) = (\mathbf{\Omega})^T$ and have following equation:

$$\dot{\mathbf{x}} = \mathbf{S}(\boldsymbol{\omega}) \mathbf{x} \quad (3.9)$$

Note that $\|\mathbf{x}\| = 1$ due to that \mathbf{x} is a column of a rotation matrix and thus has to be of unit length [7]. Denote that h is sample time and assume that the turn rate vector $\boldsymbol{\omega}(t) = \boldsymbol{\omega}_k = [\omega_{kx} \ \omega_{ky} \ \omega_{kz}]^T$ for $t \in [kh, kh+h)$ then we have the discrete time model:

$$\mathbf{x}_k = \Phi_k \mathbf{x}_{k-1} \quad (3.10)$$

where $\Phi_k = e^{\mathbf{S}(\boldsymbol{\omega}_k)h}$ has a closed form solution given by [8] $\Phi_k = \mathbf{I} + a_1 \mathbf{S}(\boldsymbol{\omega}_k)h + a_2 (\mathbf{S}(\boldsymbol{\omega}_k)h)^2$ with

$$a_1 = 1 - \frac{(\|\boldsymbol{\omega}_k\|h)^2}{3!} + \frac{(\|\boldsymbol{\omega}_k\|h)^4}{5!} - \dots$$

$$a_2 = \frac{1}{2!} - \frac{(\|\boldsymbol{\omega}_k\|h)^2}{4!} + \frac{(\|\boldsymbol{\omega}_k\|h)^4}{6!} - \dots$$

Consider \mathbf{x} as a state vector and introduce a process noise \mathbf{w} incorporating inaccuracies in modeling and gyro noise, the state transition equation is:

$$\mathbf{x}_k = \Phi_k \mathbf{x}_{k-1} + \mathbf{w}_k \quad (3.11)$$

where \mathbf{w}_k is presumed uncorrelated, zero-mean, and Gaussian with constant covariance matrix \mathbf{Q}_k .

3.2.1.1 Estimation under non-acceleration

Consider accelerometer measurement $\mathbf{f}_b = [f_{xb} \ f_{yb} \ f_{zb}]^T$ as measurement vector \mathbf{z} . When the accelerations are so low that we can consider as zero, from Equation (2.10), the measurement equation can be written:

$$\mathbf{z}_k = -\mathbf{x}_k \mathbf{g} + \mathbf{v}_k \Leftrightarrow \mathbf{z}_k = \mathbf{H} \mathbf{x}_k + \mathbf{v}_k \quad (3.12)$$

where \mathbf{v}_k is the measurement noise vector which models accelerometers noise as well as high-frequency accelerations. \mathbf{v}_k is presumed uncorrelated, zero-mean, and Gaussian with constant covariance matrix \mathbf{R}_k . And $\mathbf{H} = -\mathbf{g} \mathbf{I}_3$ is measurement matrix. The resultant Kalman-filtering equation is given by:

$$\hat{\mathbf{x}}_k = \Phi_k \hat{\mathbf{x}}_{k-1} + \mathbf{K}_k (\mathbf{z}_k - \mathbf{H} \Phi_k \hat{\mathbf{x}}_{k-1}) \quad (3.13)$$

where \mathbf{K}_k represents the Kalman gain matrix and are computed from the matrix Riccati equations given by [10]:

$$\begin{aligned} \mathbf{M}_k &= \Phi_k \mathbf{P}_{k-1} \Phi_k^T + \mathbf{Q}_k \\ \mathbf{K}_k &= \mathbf{M}_k \mathbf{H}^T (\mathbf{H} \mathbf{M}_k \mathbf{H}^T + \mathbf{R}_k)^{-1} \\ \mathbf{P}_k &= (\mathbf{I} - \mathbf{K}_k \mathbf{H}) \mathbf{M}_k \end{aligned} \quad (3.14)$$

The estimated state vector $\hat{\mathbf{x}}_k$ is not of unit length. To guarantee the constraint $\|\mathbf{x}\| = 1$ as mentioned above, we can write [7]:

$$\hat{\mathbf{x}}_k = \begin{cases} \hat{\mathbf{x}}_k / \|\hat{\mathbf{x}}_k\| & \text{if } \hat{\mathbf{x}}_k \neq \mathbf{0}, \\ \hat{\mathbf{x}}_{k-1} & \text{if } \hat{\mathbf{x}}_k = \mathbf{0}. \end{cases} \quad (3.15)$$

3.2.1.2 Estimation under acceleration

When the system is under acceleration, the measurement noise \mathbf{v}_k is large and we can set the measurement noise covariance matrix \mathbf{R}_k to infinity. Therefore, Kalman gain matrix $\mathbf{K}_k = \mathbf{0}$ and state vector is estimated as:

$$\hat{\mathbf{x}}_k = \Phi_k \hat{\mathbf{x}}_{k-1} \quad (3.16)$$

It means that when the system is under acceleration, attitude estimation is only based on rate gyros data. The same as low acceleration case, the estimated state vector is modified as:

$$\hat{\mathbf{x}}_k = \begin{cases} \hat{\mathbf{x}}_k / \|\hat{\mathbf{x}}_k\| & \text{if } \hat{\mathbf{x}}_k \neq \mathbf{0}, \\ \hat{\mathbf{x}}_{k-1} & \text{if } \hat{\mathbf{x}}_k = \mathbf{0}. \end{cases} \quad (3.17)$$

3.2.1.3 Acceleration detection

The problem is how to detect acceleration or rather, to detect non-acceleration. Recall that the accelerometer model is $\mathbf{f}_b = \mathbf{C}_n^b \mathbf{a}_n - \mathbf{x}g$. At non-acceleration state, $\mathbf{a}_n = \mathbf{0}$ and $\mathbf{f}_b = -\mathbf{x}g$, therefore, we have:

$$\|\mathbf{f}_b\| = g \|\mathbf{x}\| = g \quad (3.18)$$

It means that at non-accelerations state, the specific force \mathbf{f}_b is moving on the sphere with radius of $1g$. This condition must hold for certain amount of time before the system is considered under non-acceleration state [7].

3.2.1.4 Attitude calculation

As defined above, the state vector \mathbf{x} is the third column of rotation matrix \mathbf{C}_n^b , hence $\mathbf{x} = [-\sin \theta \cos \theta \sin \phi \cos \theta \cos \phi]^T$. From the estimated state vector $\hat{\mathbf{x}}_k = [\hat{x}_{k1} \hat{x}_{k2} \hat{x}_{k3}]^T$, we can estimate attitude as:

$$\hat{\theta}_k = \arcsin(-\hat{x}_{k1}), \quad \hat{\phi}_k = \arcsin\left(\frac{\hat{x}_{k2}}{\cos \hat{\theta}_k}\right) \quad (3.19)$$

3.2.2 Heading estimator

3.2.2.1 Estimation under homogeneous and undisturbed Earth's magnetic field

From Equation (2.6) we have:

$$\dot{\psi} = \frac{\sin \phi}{\cos \theta} \omega_y + \frac{\cos \phi}{\cos \theta} \omega_z \quad (3.20)$$

Consider ψ as state variable x and introduce a process noise w incorporating inaccuracies in modeling and gyro noise, the state transition equation is:

$$x_k = x_{k-1} + \mathbf{G}_k \mathbf{u}_{k-1} + w_k \quad (3.21)$$

where $\mathbf{G}_k = \begin{bmatrix} 0 & \frac{\sin \phi}{\cos \theta} & \frac{\cos \phi}{\cos \theta} \end{bmatrix}$, $\mathbf{u}_k = [\omega_{kx} \ \omega_{ky} \ \omega_{kz}]^T \times h$ (with h is sample time) and

w_k has variance Q_k . Note that ϕ and θ has been estimated using the attitude estimator.

From magnetometer measurement \mathbf{m}_b solve Equation (2.12) and (2.13), we have heading angle ψ_{MAG} . Consider ψ_{MAG} as measurement variable z and introduce a measurement noise v which models the magnetic sensor noise, the measurement equation is:

$$z_k = x_k + v_k \quad (3.22)$$

with v_k has variance R_k . The resultant Kalman-filtering equation is given by:

$$\hat{x}_k = \hat{x}_{k-1} + \mathbf{G}_k \mathbf{u}_{k-1} + K_k (z_k - \hat{x}_{k-1} - \mathbf{G}_k \mathbf{u}_{k-1}) \quad (3.23)$$

where K_k represents the Kalman gain and are given by:

$$\begin{aligned} M_k &= P_{k-1} + Q_k \\ K_k &= M_k (M_k + R_k)^{-1} \\ P_k &= (1 - K_k) M_k \end{aligned} \quad (3.24)$$

3.2.2.2 Estimation under non-homogeneous and disturbed Earth's magnetic field

When Earth's magnetic field is non-homogeneous and disturbed, magnetometer data are invalid and we can set the measurement noise variance R_k to infinity. Therefore, Kalman gain matrix $K_k = 0$ and state vector is estimated as:

$$\hat{x}_k = \hat{x}_{k-1} + \mathbf{G}_k \mathbf{u}_{k-1} \quad (3.25)$$

It means that when Earth's magnetic field is non-homogeneous and disturbed, heading estimation is only based on rate gyros data.

3.2.2.3 Detect homogeneous and undisturbed Earth's magnetic field

The problem is how to know whether Earth's magnetic field is homogeneous and undisturbed or not. It is based on the deviation of the magnetic field norm and the dip angle which are calculated from magnetometer data. If the magnetic vector lies on the sphere with the normalized radius of 1 and the magnetic field inclination is correct then magnetometer data is valid and Earth's magnetic field is homogeneous and undisturbed [11].

3.2.2.4 Heading calculation

From estimated state variable \hat{x}_k , we have estimated yaw angle:

$$\hat{\psi}_k = \hat{x}_k \quad (3.26)$$

Chapter 4 Simulation Studies

A set of simulation works were performed using MATLAB. In the simulation, the body is initially at $\phi = -\pi/34$, $\theta = 0$, and $\psi = 0$ and rotating about x_b -axis at angular velocity $\omega_x = 0.27 \times \sin(2 \times \pi \times 0.23 \times t) + 0.03 \times \sin(2 \times \pi \times 0.11 \times t) + 0.01 \times \sin(2 \times \pi \times 0.593 \times t)$ [rad/s] and about y_b -axis at angular velocity $\omega_y = 0.21 \times \cos(2 \times \pi \times 0.14 \times t) + 0.03 \times \cos(2 \times \pi \times 0.39 \times t) + 0.02 \times \cos(2 \times \pi \times 0.12 \times t)$ [rad/s] while $\omega_z = 0$ [rad/s].

From the above angular velocities, solve (2.6) numerically using the fourth-order Runge-Kutta method, we obtain Euler angles. Because the Euler angles are calculated from true angular velocities, we consider them as true Euler angles.

Rate gyro measurements can be simulated by adding zero-mean Gaussian white noises with $\sigma = 0.001$ [rad/s] and offset 0.005 [rad/s] to the above angular velocities. Meanwhile, accelerometer measurements are simulated by adding zero-mean Gaussian white noises with $\sigma = 0.001g$. Magnetometer measurements are simulated by the same method as the one used in Section 2.4.

The simulations have been run for 50 seconds.

In Figure 4.1, acceleration of the body and detect signal (Section 3.2.1.3) are depicted. The detect signal is used to switch the attitude estimator between non-acceleration and acceleration mode. When the detect signal is one, the attitude estimator is in non-acceleration mode. In this mode, both rate gyro data and accelerometer data are used. When the detect signal is zero, the attitude estimator is in acceleration mode. In this mode, only rate gyro data are used.

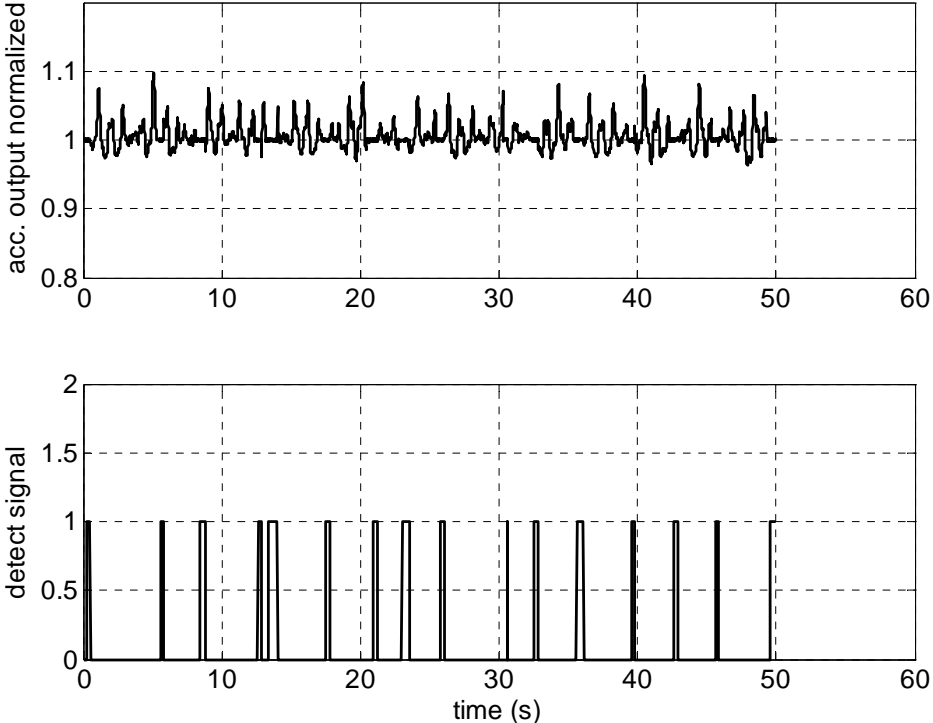


Figure 4.1 Acceleration, velocity of the body and non-acceleration detect signal.

To simulate non-homogeneous and disturbed Earth’s magnetic field, a noise vector is added to the Earth’s magnetic field vector after each 5 seconds. It makes normalized magnitude of the Earth’s magnetic field vector change as depicted in Figure 4.2. Error in dip angle and Homogeneous & undisturbed Earth’s magnetic field detect signal (Section 3.2.2.3) are also depicted. The detect signal is used to switch the heading estimator between two modes: homogeneous & undisturbed Earth’s magnetic field mode and non-homogeneous & disturbed Earth’s magnetic field mode. When the detect signal is one, the heading estimator is in homogeneous & undisturbed Earth’s magnetic field mode. In this mode, both rate gyro data and magnetometer data are used. When the detect signal is zero, the heading estimator is in non-homogeneous & disturbed Earth’s magnetic field mode. In this mode, only rate gyro data are used.

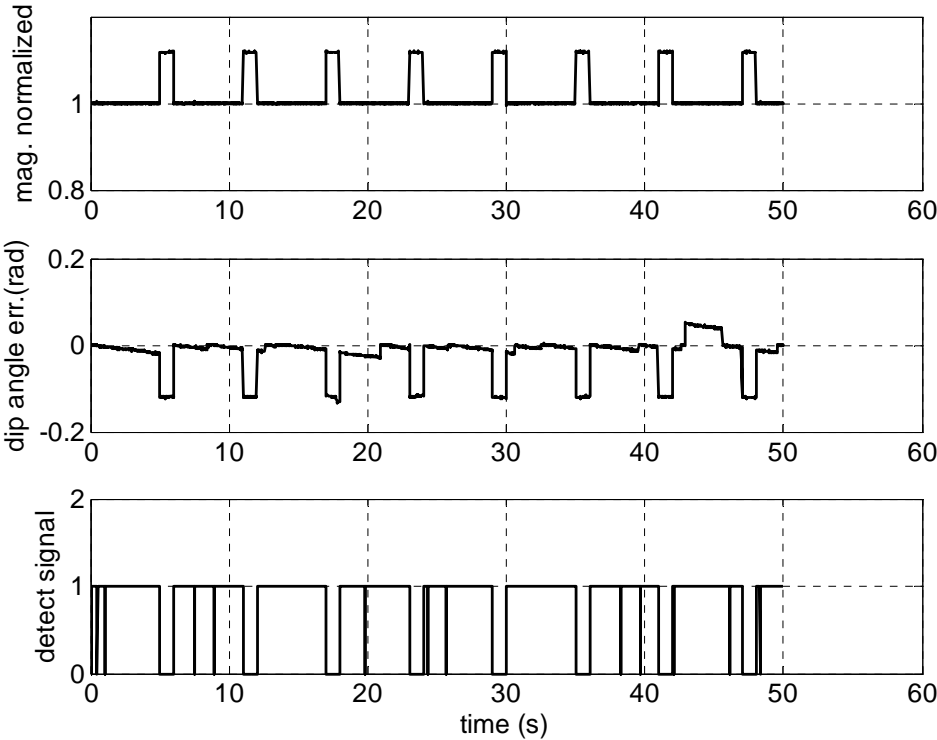


Figure 4.2 Normalized magnitude of Earth’s magnetic field, error in dip angle, and homogeneous & undisturbed Earth’s magnetic field detect signal.

Euler angles of the body are illustrated in Figure 4.3. In the figure, solid lines denote true Euler angles while dashed lines denote estimated Euler angles. We can see that there is no drift of estimated Euler angles and noises are reduced. It means that the proposed method is effective.

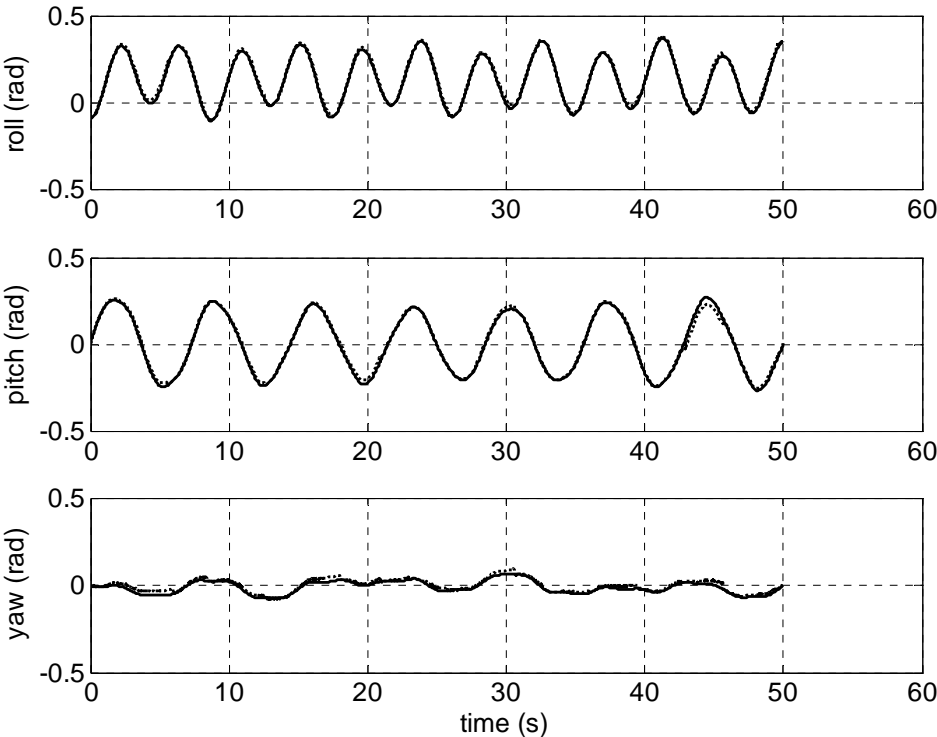


Figure 4.3 Roll, pitch, and yaw angles. Solid lines denote true values and dashed estimated.

Errors of estimated Euler angles are illustrated in Figure 4.4. There are small errors when non-acceleration detect signal is zero. However, they are reset to zeros when the detect signal is one.

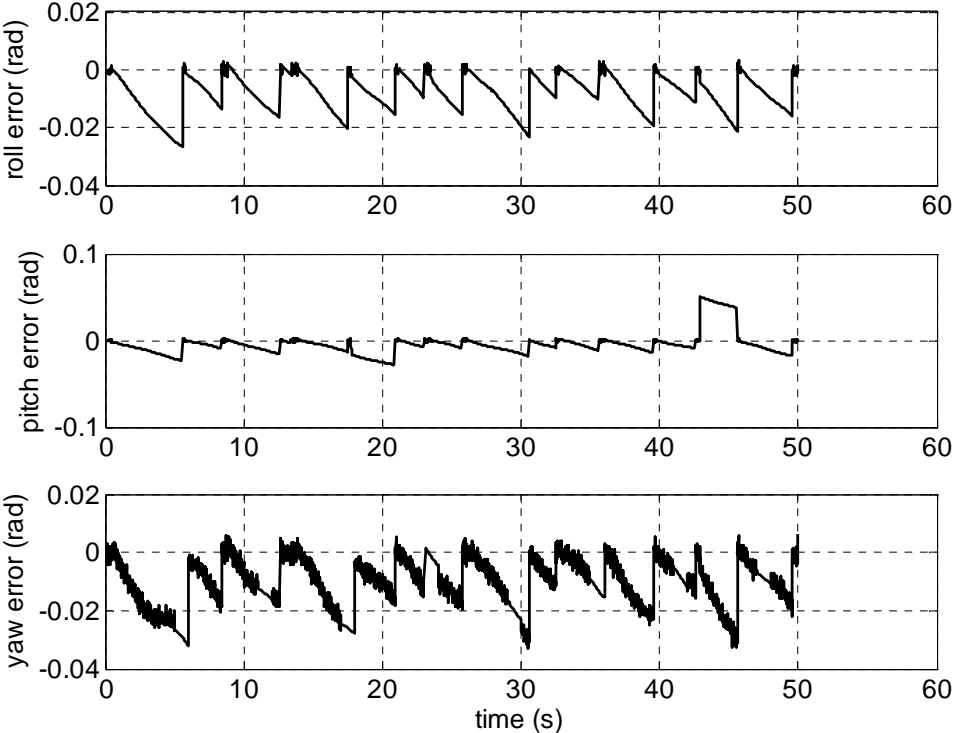


Figure 4.4 Errors in estimated roll, pitch, and yaw angles.

Elements of diagonal of estimated error covariance matrix of the attitude estimator are depicted in Figure 4.5. There is small trend of increasing errors when the attitude estimator is in acceleration mode. However, these errors are compensated for when the attitude estimator is in non-acceleration mode.

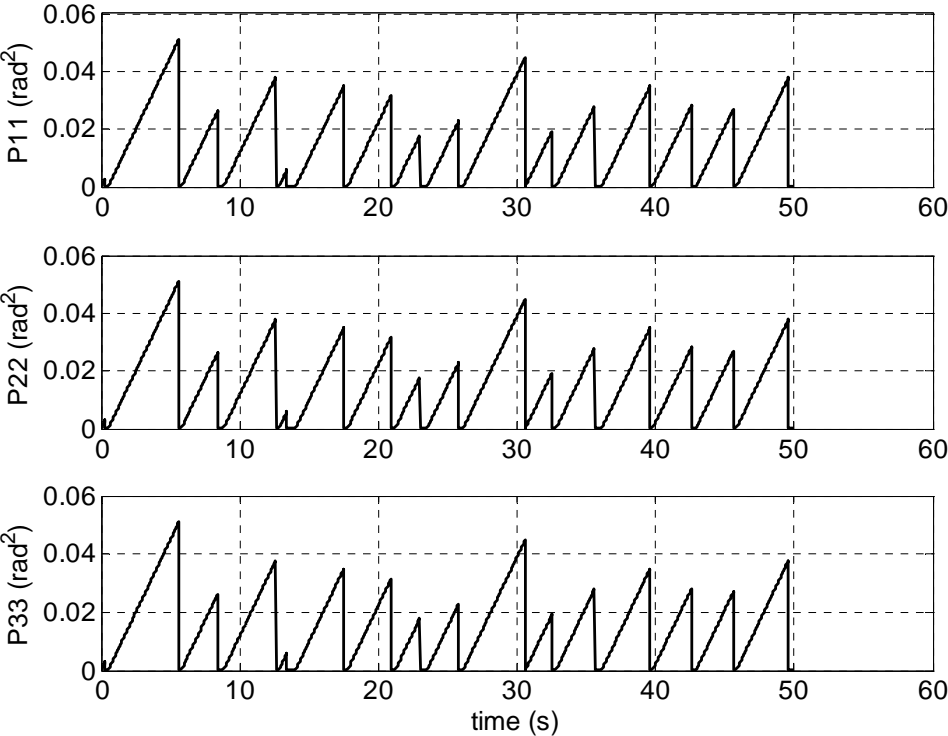


Figure 4.5 Elements of diagonal of estimated error covariance matrix of the attitude estimator.

Estimated error variance of the heading estimator is illustrated in Figure 4.6. There is small trend of increasing error when the heading estimator is in non-homogeneous & disturbed Earth's magnetic field mode. However, this error is compensated for when the heading estimator is in homogeneous & undisturbed Earth's magnetic field mode.

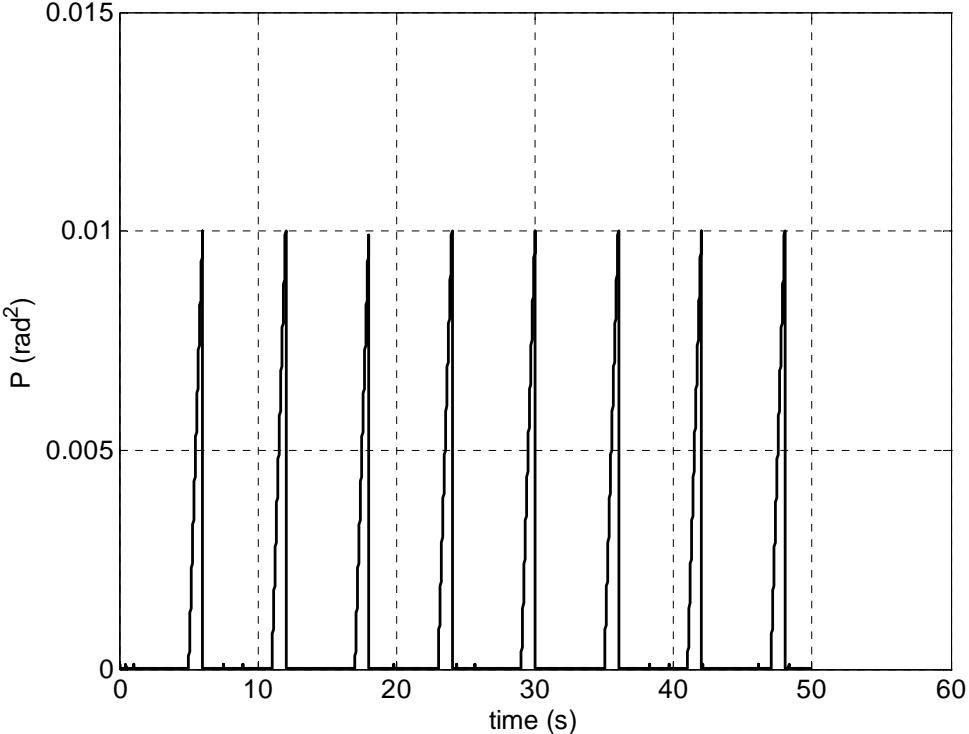


Figure 4.6 Estimated error variance of the heading estimator.

Chapter 5 Conclusions

In this paper, we have presented a methodology for designing a low-cost attitude and heading estimation system. Simulation results have shown the performance of the presented method. The method will be applied to an ROV but also can be used for other robots such as flying or climbing ones. Its low-cost, light weight, small size, and reliability makes it ideal for many robotic applications. The method uses two linear Kalman filters which makes it possible to easily obtain theoretical convergence results. It also makes the iterative computations easy to be implemented at faster rate using inexpensive microprocessors. Using the presented method, the entire rotation matrix can be estimated.

References

- [1] A. J. Baerveldt, R. Klang, “*A low-cost and low-weight attitude estimation system for a autonomous helicopter*”, in Proc. 1997 IEEE Int. Conf. on Intelligent Engineering Systems, Budapest, Hungary, pp. 391-395, 1997.
- [2] K. Loffler, M. Gienger, F. Pfeiffer, H. Ulbrich, “*Sensors and Control Concept of a Biped Robot*”, IEEE Trans. on Industrial Electronics, vol. 51, no. 5, pp. 972-980, 2004.
- [3] J. Vaganay, M. J. Aldon, A. Fournier, “*Mobile robot attitude estimation by fusion of inertial data*”, in Proc. 1993 IEEE Int. Conf. on Robotics and Automation, Atlanta, GA, USA, vol. 1, pp. 277-282, 1993.
- [4] B. Barshan, H. F. Durrant-Whyte, “*Inertial navigation systems for mobile robots*”, IEEE Transactions on Robotics and Automation, vol. 11, no. 3, 1995.
- [5] B. Barshan, H. F. Durrant-Whyte, “*Evaluation of a solid-state gyroscope for robotics applications*”, IEEE Transactions on Instrumentation and Measurement, vol. 44, no. 1, 1994.
- [6] L. Ojeda, J. Borenstein, “*FLEXnav: Fuzzy logic expert rule-based position estimation for mobile robots on rugged terrain*”, in Proc. 2002 IEEE Int. Conf. on Robotics & Automation, Washington, DC, 2002.
- [7] H. Rehbinder, X. Hu, “*Drift-free attitude estimation for accelerated rigid bodies*”, Automatica 40, pp. 653-659, 2004.
- [8] D. H. Titterton, J. L. Weston, STRAPDOWN INERTIAL NAVIGATION TECHNOLOGY, 2nd edition, American Institute of Aeronautics and Astronautics, 2004.
- [9] S. Y. Cho, C. G. Park, “*Tilt compensation algorithm for 2-axis magnetic compass*”, Electronics letters, vol. 39, no. 22, 2003.
- [10] P. Zarchan, H. Musoff, FUNDAMENTALS OF KALMAN FILTERING: A PRACTICAL APPROACH, 2nd edition, American Institute of Aeronautics and Astronautics, 2005.

- [11] D. Jurman, M. Jankovec, R. Kamnik, M. Topic, “*Calibration and data fusion solution for the miniature attitude and heading reference system*”, *Sensors and Actuators A* 138, pp. 411-420, 2007.